Rare Metal Materials and Engineering
Volume 54, Issue 4, April 2025
Available online at www.rmme.ac.cn

Science Press

Cite this article as: Xie Manman, Jia Dongxiao, Jia Xilin, et al. Annealing Treatment and Corrosion Behavior of Gd-containing Stainless Steel[J]. Rare Metal Materials and Engineering, 2025, 54(04): 871-878. DOI: https://doi.org/10.12442/j.issn.1002-185X.20240115.

ARTICLE

Annealing Treatment and Corrosion Behavior of Gd-containing Stainless Steel

Xie Manman[1,2], Jia Dongxiao[3,4], Jia Xilin[2,4], Zhao Fei[1], Liang Tian[3,5], Zhou Yangtao[2]

[1] School of Materials Science and Engineering, Taiyuan University of Science and Technology, Taiyuan 030024, China; [2] Shenyang National Laboratory for Materials Science, Institute of Metal Research, Chinese Academy of Sciences, Shenyang 110016, China; [3] Shi-Changxu Innovation Center for Advanced Materials, Institute of Metal Research, Chinese Academy of Sciences, Shenyang 110016, China; [4] School of Materials Science and Engineering, University of Science and Technology of China, Shenyang 110016, China; [5] CAS Key Laboratory of Nuclear Materials and Safety Assessment, Institute of Metal Research, Chinese Academy of Sciences, Shenyang 110016, China

Abstract: The microstructures and corrosion behavior of 1.0wt% Gd-containing neutron-absorbing duplex stainless steel annealed at different temperatures were studied. Results reveal that the content of Gd-containing secondary phase increases with increasing the annealing temperatures to 1080 ℃, and then decreases. In the sample annealed at 1080 ℃, *M*-Gd (*M*=Fe, Cr, Ni) intermetallic with M_3Gd as the core phase and M_{12}Gd as the shell is the primary secondary phase. In the sample annealed at 1140 ℃, M_3Gd phase is dominant. The corrosion behavior of the two annealed steel samples were analyzed in NaCl, HCl and H_3BO_3 solutions. It is found that the sample annealed at 1140 ℃ has lower corrosion rate. M_3Gd is more electrochemically active than M_{12}Gd when the sample is immersed in NaCl and HCl solutions, but more noble in H_3BO_3 solution.

Key words: neutron-absorbing duplex stainless steel; annealing treatment; Gd-containing intermetallics; corrosion

1 Introduction

Development of nuclear industry inevitably results in generation of a large amount of highly radioactive spent nuclear fuel (SNF) waste. During the transport and storage process of SNF, neutron-absorbing structural materials are widely used for the containers, racks and transport parts[1–3]. Fe-based[4–7], Ni-based[8–11] alloys and Al-matrix composites[12–16] containing neutron-absorbing elements are the most commonly used materials. For wet-storage method, SNF should be immersed in B acid solution for years. Therefore, corrosion resistance of the neutron-absorbing materials, in addition to their strength, ductility and processing ability, should be seriously considered.

Fe-based and Ni-based alloys, particularly stainless steels (SSs), are the most prominent candidates for this application. Among them, B-containing SSs have been used widely. However, the shortage of the material is obvious: on the one hand, the limited solubility of B in SSs prevents the production of alloys with B content more than 2.25wt%[17]; on the other hand, the ductility of the early borated SS decreases with increasing the volume fraction of B-containing secondary phases[18]. Additionally, He gas bubbles will be generated in B-containing metals by long-term neutron irradiation, which is a safety risk for structural materials[19]. In recent years, Gd-containing alloys have received increasing attention due to their superior thermal neutron absorption ability and free of He generation. The thermal neutron absorption cross-sections of ^{155}Gd and ^{157}Gd are 16 and 66 times higher than those of ^{10}B, respectively[20–21]. A series of Gd-containing Fe and Ni alloys have been used and studied in the past decades, and Gd-containing steels are particularly preferred from the economic consideration[22]. Since Gd has a very low solubility limit in the Fe- and Ni-based matrices, it usually presents in the form of Gd-containing secondary phases, which significantly influence the corrosion resistance and mechanical properties

Received date: April 05, 2024
Foundation item: Research Foundation of Shenyang National Laboratory for Materials Science (L2019F15); Ling Chuang Research Project of China National Nuclear Corporation (CNNC-LCKY-202279)
Corresponding author: Zhou Yangtao, Ph. D., Professor, Shenyang National Laboratory for Materials Science, Institute of Metal Research, Chinese Academy of Sciences, Shenyang 110016, P. R. China, E-mail: ytzhou@imr.ac.cn

of the alloys[6,11,23–24]. M_3Gd, M_5Gd and $M_{17}Gd_2$ are common secondary phases in Gd-containing steels[25–26].

The types of metallic *M*-Gd phases are closely related to compositions and heat-treatment process of the steel matrix[27]. Kang et al[6] designed three Gd-containing alloy steels and found a new type of precipitate, M_{12}Gd, which has a higher melting temperature than other precipitates, suggesting that it can be utilized for alloys with better hot workability and weldability. Wang et al[28] studied the effect of solution treatment temperatures on the secondary phase and hardness of Gd-SS, and found that the "gray" phase was wrapped with "bright white" phase. After solid solution treatment at 1000–1070 ℃, the "bright white" phase gradually transformed into "gray" phase.

Moreover, the corrosion resistance of the steels is also highly influenced by the Gd-containing phases. In Gd-316 SS, $(Fe, Cr, Ni)_3Gd$ is usually found along grain boundaries. The precipitation of $(Fe, Ni, Cr)_3Gd$ will result in a Cr-rich and Ni-poor zone in the steel, thus destroying the stability of the matrix[29]. Lister et al[8] found that the preferential dissolution of Gd-containing intermetallics reduced the corrosion resistance of the steel matrix. However, it was also reported that the addition of a small amount of Gd to mild steels and duplex SSs was conducive to the corrosion resistance improvement of the steel[30].

In the present study, a 1.0wt% Gd-containing duplex SS was prepared. The material was annealed at different temperatures and the secondary phases in these samples were investigated. In addition, the corrosion resistance related to the intermetallics was studied in various aqueous conditions. This research is believed to provide fundamental knowledge for the design and fabrication of Gd-containing alloys used for SNF transport and storage.

2 Experiment

2.1 Material

The test material was Gd-containing duplex SS produced by vacuum induction melting process. The cast ingot weighted about 20 kg with a diameter about 150 mm. The composition of duplex SSs was determined by inductively coupled plasma-mass spectrometry (ICP-MS, 8900 Agilent), and the content of carbon and oxygen was determined by Carbon/Sulfur analyzer (CS844, Leco) and Oxygen/Nitrogen & Hydrogen analyzer (ONH836, Leco), respectively. The chemical composition of the as-cast steel is listed in Table 1.

In the temperature range between 1060 and 1140 ° C, a series of heat-treatment conditions were tested. The samples annealed at 1080 and 1140 ° C, named as 1080 and 1140, respectively, for 30 min showed the most pronounced difference in the volume fraction of secondary phases and were finally chosen for investigation. The samples with size of 10 mm×10 mm×10 mm were cut from the center of the obtained duplex SS.

Table 1 Chemical composition of Gd-containing duplex SS (wt%)

Cr	Ni	Mo	Mn	Si	C	O	Gd	Fe
23.7	8.2	1.2	1.6	0.4	0.024	0.0034	1.0	Bal.

2.2 Microstructural characterization

The samples were mechanically ground using SiC abrasive paper from 400# to 2000#, and polished using a water-based diamond suspension containing 2.5 μm particles to obtain a mirror finish. The microstructures of the steel samples were analyzed by scanning electron microscope (SEM, Zeiss-Supra 35). Chemical composition of the secondary phase and matrix was analyzed by energy dispersive spectroscope (EDS) attached to SEM. The phase distribution was characterized using an X-ray diffractometer (XRD) with Cu Kα radiation (Rigaku Ultima IV, Japan), under parameters of 30 kV, 15 mA, λ = 0.15406 nm, and 2θ=40°–100°. The area fraction of the secondary phase was analyzed using ImageJ software. A Thermo Fisher Talos F200X transmission electron microscope (TEM) was used to determine the crystallographic information of the Gd-containing phases. TEM sample discs with 3 mm in diameter were ground using silicon carbide papers, then dimpled and finally thinned by ion-milling system Gatan PIPS 695.

2.3 Corrosion test

Potentiodynamic polarization tests were carried out with an electrochemical workstation (Gamry Reference 600+). The standard three-electrode system was used with the saturated calomel electrode as the reference electrode, the platinum electrode as the auxiliary electrode, and the packaged sample as the working electrode. The sample (10 mm×10 mm×1 mm) for the working electrode was connected to Cu wire and cold mounted by epoxy resin. The exposed area of the working electrode was controlled to 1 cm^2. The mounted samples were ground by SiC paper up to 2000#. The corrosion tests were repeated at least 3 times for each sample to confirm the reproducibility of the experiment.

Corrosion behavior of the Gd-containing duplex SSs was examined through potentiodynamic polarization tests. For the polarization tests, 0.1 μg/L NaCl solution[9,31–32], 0.36 mol/L HCl solution[33] (pH≈0.44) and H_3BO_3 solution[12,34] with 2.7×10^6 μg/L B (pH≈4.88) were used. H_3BO_3 solution was used to simulate spent fuel pool environment. NaCl and HCl solutions were used to investigate the polarization behavior of the samples in a neutral Cl^--containing solution and a solution with low pH.

In addition, the corrosion resistance of the samples was also studied by immersion tests in NaCl, HCl and H_3BO_3 solutions. The steel samples were mechanically ground by SiC abrasive paper up to 2000#, and polished by a water-based diamond suspension containing 2.5 μm particles to obtain a mirror finish. After corrosion tests, the corrosion morphologies were examined by SEM. Table 2 summarizes the corrosion conditions.

3 Results and Discussion

3.1 Microstructures

The as-cast Gd-containing duplex SS and the samples

Table 2 Test conditions for potentiodynamic polarization and immersion tests

Potentiodynamic polarization test	Immersion test
0.1 μg/L NaCl, 25±1 °C	0.1 μg/L NaCl, 40±1 °C, 10 h
0.36 mol/L HCl, 25±1 °C	0.36 mol/L HCl, 40±1 °C, 4 h
H_3BO_3 (B content: 2.7×10^6 μg/L), 25±1 °C	H_3BO_3 (B content: 2.7×10^6 μg/L), 40±1 °C, 3 h

annealed at 1080 and 1140 ℃ for 30 min were firstly analyzed by XRD, as shown in Fig. 1. XRD results indicate that the phase composition in the samples annealed at different temperatures all includes α-ferrite, γ-austenite and Gd-containing phases. The characteristic diffraction peaks of α-steel, i. e. $(110)_\alpha$, $(200)_\alpha$ and $(211)_\alpha$, and the peaks of γ-phase i. e. $(111)_\gamma$, $(200)_\gamma$, $(311)_\gamma$ and $(220)_\gamma$, can be clearly seen.

SEM-BSE images of the steels are displayed in Fig. 2. The production of back-scattered electrons differs based on the mass of the element, so BSE image is generally used to reveal the distribution of various elements in samples. Gd has a relatively higher atomic mass than other elements in the steel. According to the contrast difference, the bright Gd-containing phase can be easily distinguished from the steel matrix. In the matrix, the two steel phases are also distinguishable, i. e. the dark grey matrix is the α-ferrite phase and the light grey one is the γ-austenite phase. The γ-austenite is continuously long and elliptically distributed on the continuous α-ferrite phase. It is worth noting that the Gd-containing secondary phases can be classified into two types: single-phase particles and dual phases (core-shell structure) particles. In the latter particle, the central part possesses higher contrast, indicating Gd-rich compound.

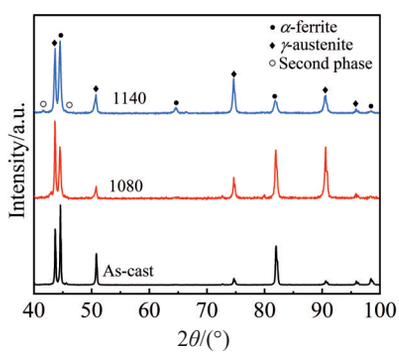

Fig.1 XRD patterns of as-cast steel and annealed samples

According to Fig. 3, the content of Gd-containing particles in the sample 1080 is about 7.12%, which is higher than that in the as-cast sample and sample 1140. Fig. 2d−2f reveal that most of the secondary phases in the as-cast sample is Gd-rich phase and the dual-phase particles with Gd-rich core are dominant in sample 1080. However, when the annealing temperature is set to 1140 ℃ , the Gd-lean phases are transformed to Gd-rich ones. The particle size statistically decreases and the smaller ones are mainly Gd-rich phases. Only a small fraction of the particles show a thin Gd-lean fringe. The area fraction of the two types of *M*-Gd phases are measured and given in Fig. 4a. In addition, the area fraction of the α and γ phases in the steel matrix are measured as well (Fig. 4b). The area fraction of γ phase in the matrix decreases from 62% to about 48% with the increase in annealing temperature.

To determine the chemical composition of the Gd-

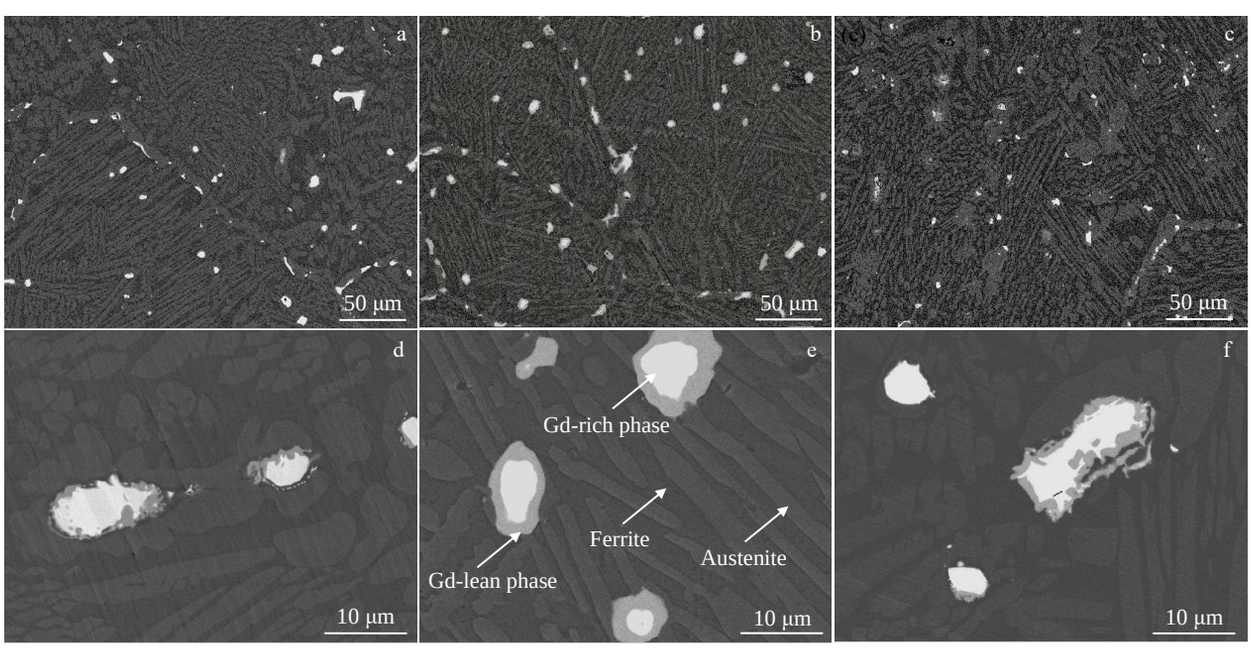

Fig.2 SEM-BSE images of as-cast steel (a, d), sample 1080 (b, e), and sample 1140 (c, f)

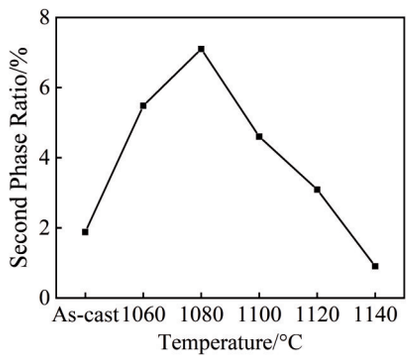

Fig.3 Area fractions of Gd-containing particles in the steel annealed at different annealing temperatures

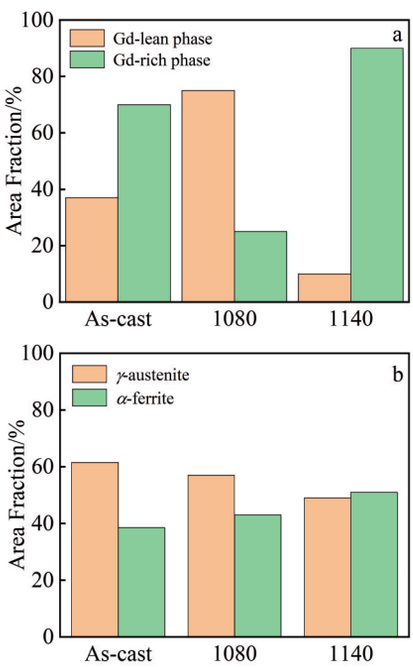

Fig.4 Quantitative analysis on area fractions of Gd-containing phases (a) and matrix (b) in the three steel samples

containing compounds, EDS analysis was performed on each sample. The constituent elements and atomic ratio of the two secondary phases and matrix are given in Table 3. The values in Table 3 are the average of 3 individual samples. Gd is not detected in the matrix, which is mainly enriched with elements Fe, Cr and Ni. The two secondary phases with different contrasts are mainly composed of elements Fe, Cr, Ni, Gd, Mn and Si. The Gd-rich phase is enriched with Ni and the Gd-lean phase is rich in Fe and Cr. According to the atomic ratio of (Fe+Ni+Cr)/Gd, the white Gd-rich phase is estimated to be M_3Gd, where M denotes transition metallic elements, and the grey white compound is determined as M_{12}Gd or M_{11}Gd.

To determine the crystallographic structures of the two Gd-containing intermetallics, the steel samples were characterized by TEM. Fig. 5 shows TEM micrograph and selected-area electron diffraction (SAED) patterns of Gd-containing compounds. A tetragonal structure with lattice parameters of a=0.86 nm and c=0.48 nm can be determined according to Fig. 5b. Judged by the lattice parameters and the chemical composition, the Gd-lean phase can be determined as M_{12}Gd phase[6]. The diffraction pattern acquired from the Gd-rich phase is shown in Fig. 5c. The crystalline structure of the compound is in line with M_3Gd which is a hexagonal phase[6,35]. EDS mapping under TEM platform was also carried out to investigate the composition distributions in the two Gd-phases. As shown in Fig. 6, the phase boundary area is analyzed. EDS results confirm the enrichment of Fe and Cr in the M_{12}Gd phase and the Ni-enrichment in M_3Gd.

3.2 Corrosion behavior

Since the compositional and structural inhomogeneity in the as-cast steel often induce the uncertainty of corrosion data, only the annealed steel samples were tested and compared in this section. Potentiodynamic polarization curves of the annealed SS measured in a 0.1 μg/L NaCl solution are shown in Fig. 7a. The current peaks, such as the ones at 0.06 and 0.27 V_{SCE}, are attributed to dissolution of the Gd-containing secondary phases[8,36]. The two samples in the dilute NaCl solutions do not exhibit active-passive transition.

The corrosion potential E_{corr}, corrosion current I_{corr} and the calculated corrosion rate V_{corr} are summarized in Table 4. The E_{corr} of the sample 1140 determined by the polarization curve is approximately −0.146 V_{SCE}, which is slightly higher than the value of sample 1080. Since the Gd-containing phases are more electrochemically active than steel matrix, it is reasonable that the steels containing more M-Gd intermetallics show higher corrosion current in the anodic region.

Fig. 7b shows the potentiodynamic polarization curves of the alloys in a 0.36 mol/L HCl solution at 25 °C. The anodic current is three or four orders of magnitude larger than the values measured in other solutions. The current is contributed by the severe dissolution of secondary M-Gd phases in HCl solution. At the potentials larger than −0.3 V_{SCE}, the samples exhibit passivity and uniform corrosion of the steel matrix.

Table 3 Chemical composition of steel matrix and Gd-containing secondary phases

Position	wt%				at%				Atomic ratio of (Fe+Ni+Cr)/Gd
	Fe	Ni	Cr	Gd	Fe	Ni	Cr	Gd	
Core	17.84	36.98	3.04	46.56	18.48	32.53	3.98	18.13	3.03
Shell	44.90	16.33	14.03	19.53	44.91	11.59	16.69	6.31	11.59
α-ferrite	62.46	7.99	22.78	-	53.22	6.47	20.85	-	-
γ-austenite	61.09	5.73	25.85	-	51.07	4.56	23.21	-	-

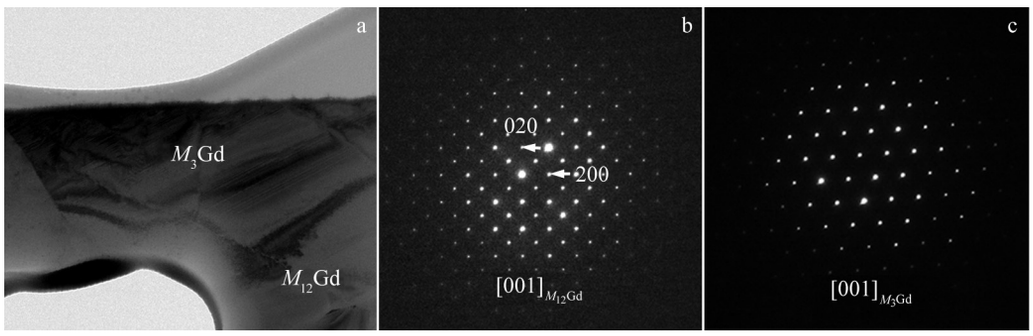

Fig.5 TEM image of dual-phase compound (a); SAED patterns of M_{12}Gd (b) and M_3Gd (c) phases

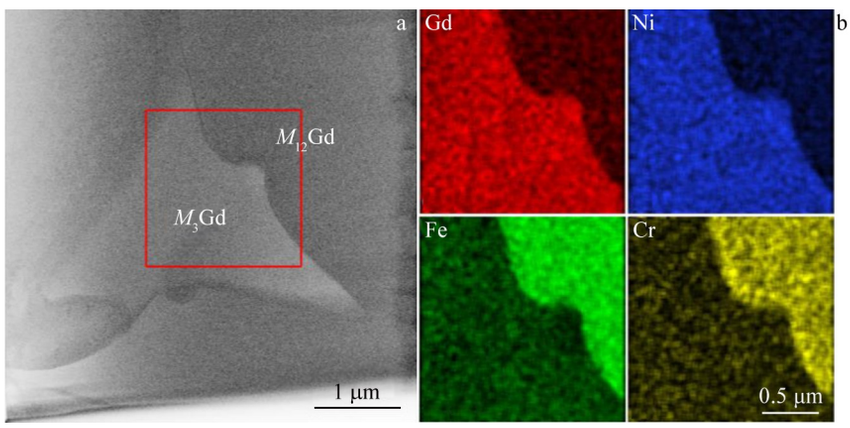

Fig.6 TEM image (a) and corresponding EDS mappings of a dual-phase intermetallic marked by rectangle in Fig.6a (b)

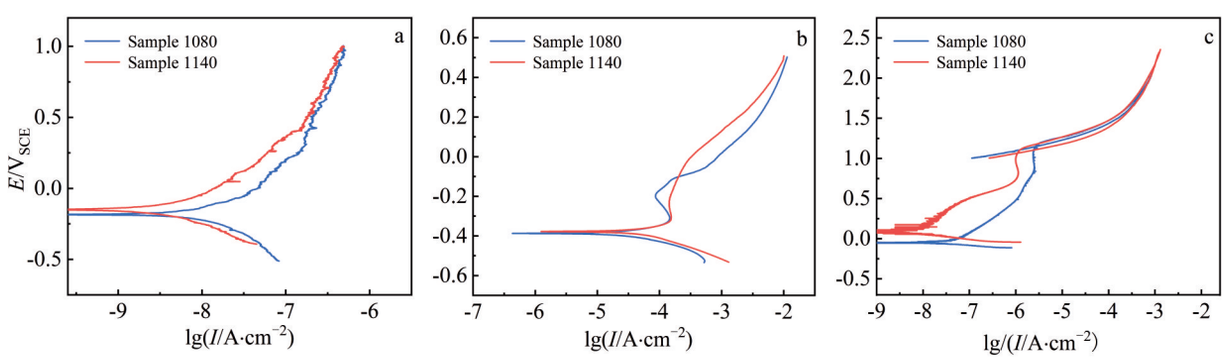

Fig.7 Potentiodynamic polarization curves of annealed steels in different solutions: (a) 0.1 μg/L NaCl, (b) 0.36 mol/L HCl, and (c) H_3BO_3 (B content: 2.7×10^6 μg/L)

After the passivity region, the sample 1080 also shows higher corrosion current, which indicates that the corrosion rate of the steel in HCl solution is determined by the content of *M*-Gd phase.

To evaluate the practical corrosion resistance of the duplex SS, it was also tested in H_3BO_3 (B=2.7×10^6 μg/L) solution. The polarization curves are shown in Fig.7c. In this solution, the two samples exhibit active-passive transition as well. In the range from open-circuit potential to passivation voltage, the alloys show active dissolution. When the applied voltage is increased to 0.8 V, passivation occurs. The fitting results shown in Table 4 indicate that the sample 1140 is more corrosion-resistant in H_3BO_3 solution. Compared with the results in other two solutions, the difference in E_{corr} and I_{corr} between the samples 1080 and 1140 in H_3BO_3 is the largest.

Table 4 Fitting and calculation results based on potentiodynamic polarization curves

Sample	E_{corr}/V$_{SCE}$	I_{corr}/A·cm^{-2}	V_{corr}/g·m^2·h^{-1}
1080 in NaCl solution	−0.182	4.148×10^{-9}	2.887×10^{-5}
1140 in NaCl solution	−0.146	1.023×10^{-9}	0.712×10^{-5}
1080 in HCl solution	−0.386	4.073×10^{-5}	0.281
1140 in HCl solution	−0.376	2.634×10^{-5}	0.183
1080 in H_3BO_3 solution	−0.042	6.501×10^{-8}	4.331×10^{-4}
1140 in H_3BO_3 solution	0.091	2.153×10^{-8}	1.432×10^{-4}

The corrosion morphologies of the alloys subjected to immersion tests in various solutions were characterized by SEM. Fig.8 presents SEM images of the samples immersed in a NaCl solution for 10 h. In the two alloys, corrosion initiation occurs at the Gd-containing phases, while the steel matrix remains intact. According to Fig.8b and 8d, it is found that the M_3Gd phase (core part) is more vulnerable to corrosion than the M_{12}Gd phase (shell part). Therefore, the dissolution of Gd-containing particles is almost at the center area.

Fig.9 shows the corroded surfaces of the samples immersed in 0.36 mol/L HCl solution for 4 h. For the sample 1080 subjected to immersion in the acid solution with Cl^-, the M_3Gd core is preferentially dissolved in some core-shell particles, while some other particles are entirely dissolved. However, for sample 1140, almost all the *M*-Gd particles are completely corroded. The preferential dissolution of Gd-rich phase is reasonable since the standard electrode potential of Gd (−2.279 V versus standard hydrogen electrode[37]) is much lower than

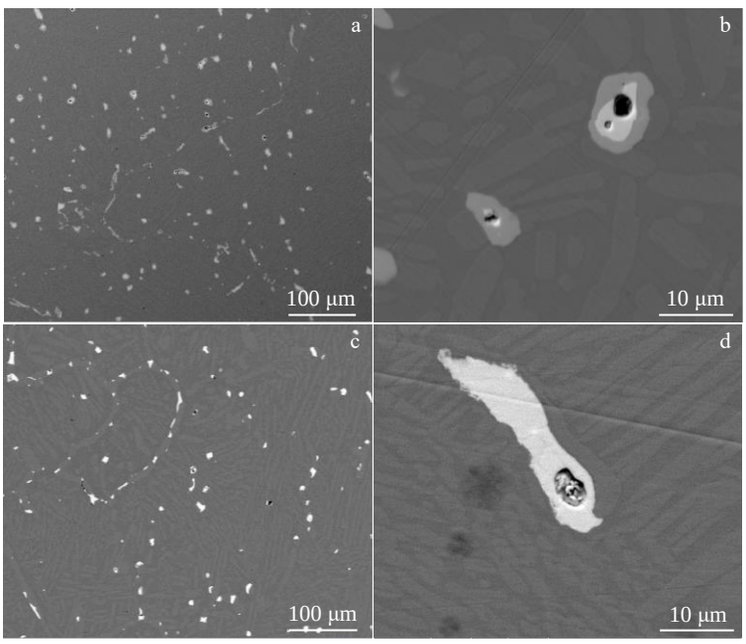

Fig.8 SEM images of corrosion morphologies of annealed steels immersed in 0.1 μg/L NaCl solution at 40 °C for 10 h: (a–b) sample 1080; (c–d) sample 1140

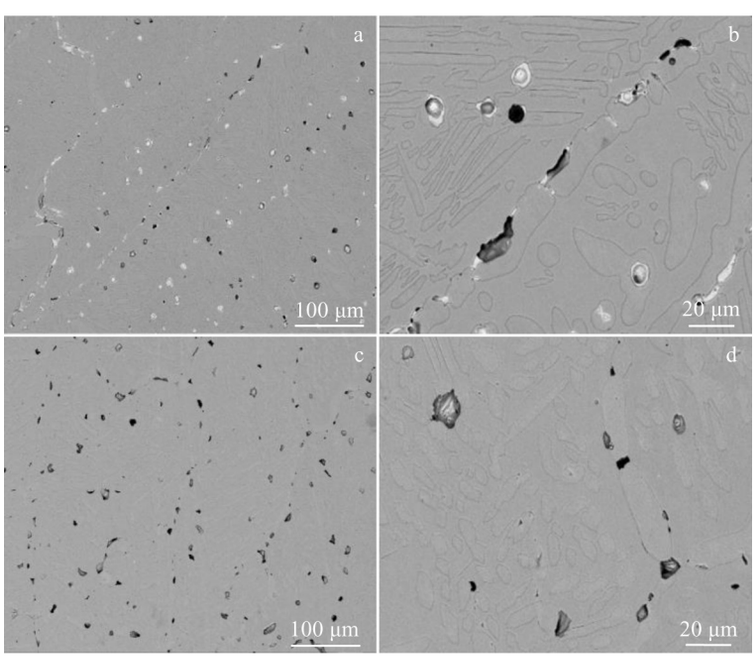

Fig.9 SEM images of corrosion morphologies of annealed steels immersed in 0.36 mol/L HCl solution at 40 ℃ for 4 h: (a–b) sample 1080; (c–d) sample 1140

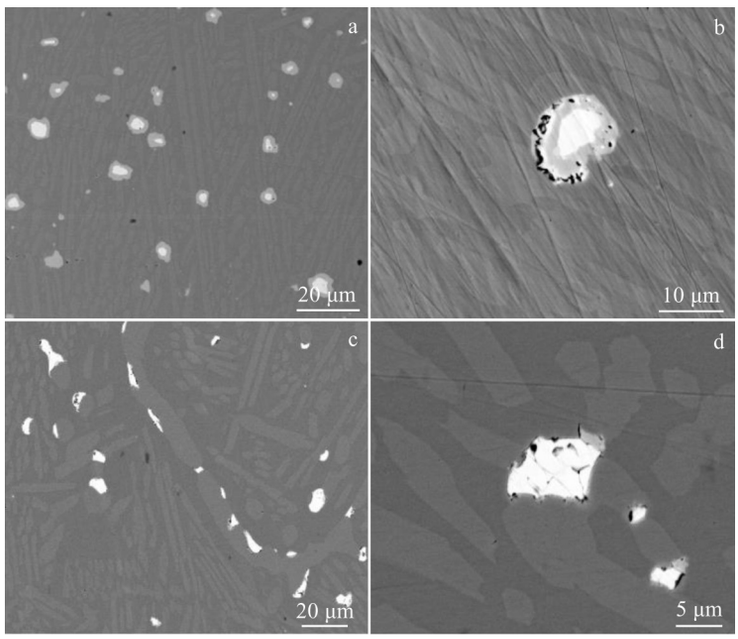

Fig.10 SEM images of corrosion morphologies of annealed steels immersed in H_3BO_3 solution (B content: 2.7×10^6 μg/L) at 40 ℃ for 3 h: (a–b) sample 1080; (c–d) sample 1140

other elements in the steel matrix. Gd can form hydroxide ($Gd(OH)_3$) in alkaline solution, but it is difficult to form a stable oxidative protective film in neutral and acidic environments[37]. From a mechanistic perspective, the corrosion rates of the steel samples are mainly determined by the exposed *M*-Gd intermetallics on steel surface, since they act as weak points disrupting the continuity of passive film. During the corrosion process, dissolution of *M*-Gd phases leads to the exposure of fresh metal matrix and the following pitting initiation. In HCl solution, the steel matrix also suffered corrosion attack. Some of the dissolution pits are extended into the steel matrix, initiating pitting corrosion (Fig.9b). The microstructure of the Gd-containing phases may have an influence on the corrosion behavior, especially the corrosion resistance of the steel. The partial dissolution of the *M*-Gd phases with core-shell structure is the evidence, and underlying mechanism warrants further investigation in the future.

The corroded surface morphology of the two alloys immersed in H_3BO_3 (B content: 2.7×10^6 μg/L) solution was examined by SEM as well. As shown in Fig. 10, it is worth noting that most of the *M*-Gd particles are not dissolved. A close inspection indicates that dissolution preferentially occurs in $M_{12}Gd$ phase (shell part), which is significantly different from the corrosion behavior of the steels in NaCl and HCl solutions. This phenomenon is consistent with findings by Ha et al[38]. In their work, the Gd-lean phase ($(Fe, Ni)_{17}Gd_2$) showed more severe corrosion morphology after immersion in H_3BO_3 solution (B content: 1.78×10^6 μg/L) for 3 h. The preferential dissolution of Gd-lean phase in H_3BO_3 solution is due to the affinity between the H_3BO_3 and Gd[39]. In the H_3BO_3 solution (pH<7), the Gd-containing phase can be protected due to the selective adsorption of H_3BO_3 to *M*-Gd phase and such adsorption appears to provide enhanced protection for the Gd-rich phase. This factor may also account for the relatively large difference in the electrochemical corrosion rates between the two alloys in H_3BO_3 solution, as shown in Table 4.

4 Conclusions

1) Two types of Gd-containing phases, M_3Gd and $M_{12}Gd$, are identified in Gd-containing duplex stainless steels. As the annealing temperature increases, the content of Gd-containing phases increases firstly and then decreases. Core-shell structured *M*-Gd intermetallics and the Gd-rich phase (M_3Gd) are dominant secondary phases in the sample 1080 and sample 1140, respectively.

2) The corrosion rate of the steels is related to the content of *M*-Gd intermetallics. The sample 1140 shows better corrosion resistance than the sample 1080.

3) M_3Gd phase is more electrochemically active than $M_{12}Gd$ in NaCl and HCl solutions, but more noble in H_3BO_3 solutions.

References

1 Soliman S E, Youchison D L, Baratta A J *et al. Nuclear Technology*[J], 1991, 96(3): 346

2 Hu Xiaogang, Du Chengjie, Pan Xiaolong *et al. Materials China*[J], 2024, 43(2): 151 (in Chinese)

3 Li Aodi, Liang Tian, Zhang Xueliang *et al. Rare Metal Materials and Engineering*[J], 2024, 53(3): 736 (in Chinese)

4 Robino C V, Michael J R, DuPont J N *et al. Journal of Materials Engineering and Performance*[J], 2003, 12: 206

5 Jung M Y, Baik Y, Choi Y *et al. Nuclear Engineering and*

Technology[J], 2019, 51(1): 207
6 Kang J Y, Jang J H, Kim S D *et al. Journal of Nuclear Materials*[J], 2020, 542: 152462
7 Stoulil J, Hemmer V, Šefl V *et al. Materials and Corrosion*[J], 2015, 66(4): 342
8 Lister T E, Mizia R E, Pinhero P J *et al. Corrosion*[J], 2005, 61(7): 706
9 Mizia R E, Lister T E, Pinhero P J *et al. Nuclear Technology*[J], 2006, 155(2): 133
10 Mizia R E, Lister T E. *Nuclear Technology*[J], 2011, 176(1): 9
11 DuPont J N, Robino C V, Michael J R *et al. Welding Journal*[J], 2004, 83(11): 289
12 Zhou Y T, Zan Y N, Wei X X *et al. Corrosion Science*[J], 2019, 153: 74
13 Zhou Y T, Zan Y N, Wang Q Z *et al. Corrosion Science*[J], 2020, 174: 108808
14 Zan Y N, Zhang Q, Zhou Y T *et al. Journal of Nuclear Materials*[J], 2019, 526: 151788
15 Chen Hongsheng, Wang Wenxian, Nie Huihui *et al. Rare Metal Materials and Engineering*[J], 2020, 49(12): 4358 (in Chinese)
16 Chen Hongsheng, Wang Wenxian. *Rare Metal Materials and Engineering*[J], 2017, 46(2): 392 (in Chinese)
17 Choi Y, Moon B M, Sohn D S. *Nuclear Engineering and Technology*[J], 2013, 45(5): 689
18 Cetin M, Ölmez E. *Protection of Metals and Physical Chemistry of Surfaces*[J], 2020, 56: 619
19 Gu Mingfei, Huang Dagui, Zhao Yong *et al. Rare Metal Materials and Engineering*[J], 2022, 51(12): 4726 (in Chinese)
20 Ho S L, Yue H, Tegafaw T *et al. ACS Omega*[J], 2022, 7(3): 2533
21 Kang Y R, Lee M W, Kim G N. *Nuclear Science and Engineering*[J], 2015, 180(1): 86
22 Lee S W, Ahn J H, Moon B M *et al. Materials & Design*[J], 2020, 194: 108906
23 Zhang W, Li C, Su X. *Journal of Phase Equilibria*[J], 1998, 19(1): 56
24 Saidi M, Walha S, Nouri K *et al. Journal of Alloys and Compounds*[J], 2019, 792: 87
25 Zhang Cheng, Pan Jie, Wang Zixie *et al. Nuclear Engineering and Technology*[J], 2023, 55(5): 1541
26 Qi Z D, Yang Z, Meng X F *et al. Materials Today Communications*[J], 2023, 37: 107315
27 Andersson J O, Helander T, Höglund L *et al. Calphad*[J], 2002, 26(2): 273
28 Wang Yurong, Wu Yu, Li Yongwang *et al. Heat Treatment of Metals*[J], 2023, 48(2): 200 (in Chinese)
29 Qi Zhengdong, Yang Zhong, Li Jianping *et al. Materials*[J], 2022, 15(9): 3255
30 Khan Z. *Journal of the Southern African Institute of Mining and Metallurgy*[J], 2012, 112(4): 309
31 Ha H Y, Jang J H, Lee T H *et al. Corrosion Science*[J], 2021, 192: 109798
32 Ha H Y, Kim S D, Jang J H *et al. Journal of The Electrochemical Society*[J], 2020, 167(10): 101506
33 Mizia R E, Lister T E, Pinhero P J *et al. Nuclear Technology*[J], 2006, 155(2): 133
34 Zhang Shenghan, Lu Quan, Xu Yunfei *et al. International Journal Electrochemical Science*[J], 2018, 13: 3246
35 Pan Jie, Wang Zixie, Mei Qiliang *et al. Scripta Materialia*[J], 2023, 234: 115575
36 Mizia R E, Lister T E, Pinhero P J *et al. Corrosion 2003*[C]. California: Nace Corrosion, 2003: NACE-03679
37 Murphy G W. *Science*[J], 1966, 154(3756): 1537
38 Ha H Y, Lee T H, Jo H H *et al. Journal of Nuclear Materials*[J], 2023, 578: 154367
39 Horkans J. *Journal of the Electrochemical Society*[J], 1979, 126(11): 1861

含Gd不锈钢的时效处理及腐蚀行为

解曼曼[1,2]，贾洞箫[3,4]，贾茜霖[2,4]，赵　菲[1]，梁　田[3,5]，周杨韬[2]
(1. 太原科技大学 材料科学与工程学院，山西 太原 030024)
(2. 中国科学院金属研究所 沈阳材料科学国家研究中心，辽宁 沈阳 110016)
(3. 中国科学院金属研究所 师昌绪先进材料创新中心，辽宁 沈阳 110016)
(4. 中国科学技术大学 材料科学与工程学院，辽宁 沈阳 110016)
(5. 中国科学院金属研究所 核用材料与安全评价重点实验室，辽宁 沈阳 110016)

摘　要：研究了含1wt% Gd中子吸收双相不锈钢在不同温度时效后的微观结构与腐蚀行为。结果表明，材料中含Gd第二相的体积比以1080 ℃为转折点，先增后减。在1080 ℃时效处理的样品中，主要以第二相为双相*M*-Gd化合物（*M*=Fe，Cr，Ni），其核心为M_3Gd相，外层为M_{12}Gd相。在1140 ℃时效处理后，M_3Gd为主要第二相。同时，研究了这两种样品在NaCl、HCl及H_3BO_3溶液中的腐蚀行为。1140 ℃处理后的样品具有相对较低的腐蚀速率。在NaCl和HCl溶液中，M_3Gd较M_{12}Gd具有较高的电化学活性；而在H_3BO_3溶液中，M_3Gd则较为稳定。

关键词：中子吸收双相不锈钢；时效处理；含Gd金属间化合物；腐蚀

作者简介：解曼曼，女，1998年生，硕士生，太原科技大学材料科学与工程学院，山西 太原 030024，E-mail：tyustxmm@163.com